Simple model for chain packing and crystallization of soft colloidal polymers

Robert S. Hoy*
Department of Physics, University of South Florida, Tampa, Florida 33620, USA

Nikos Ch. Karayiannis
Institute for Optoelectronics and Microsystems (ISOM) and ETSII, Universidad Politécnica de Madrid, Madrid, Spain
(Received 10 May 2013; published 2 July 2013)

We study a simple bead-spring polymer model exhibiting competing crystallization and glass transitions. Constant-pressure molecular dynamics simulations are employed to study phase behavior and morphological order. For adequately slow quench rates, chain systems exhibit a first-order phase transition (crystallization) below a critical temperature $T = T_{\mathrm{cryst}}$. We observe the formation of close-packed crystallites of FCC and/or HCP order, separated by domain walls, twin defects, and amorphous regions. Such crystal structures closely resemble the corresponding ordered morphologies of athermal polymer packings: fully flexible chains retain random-walk-like configurations in the crystalline state and do not form lamellae, while semiflexible chains do form lamellae. The model presented here is well suited to the modeling of granular and colloidal polymers, in particular for elucidating the factors that dictate the formation of specific ordered morphologies.

DOI: 10.1103/PhysRevE.88.012601 PACS number(s): 61.41.+e, 64.70.km, 64.60.Cn, 64.70.dg

I. INTRODUCTION

Recent years have seen an explosion of interest in colloidal and granular systems composed of polymerized chains [1–11]. Particular emphasis has been placed on how chain stiffness and molecular topology affect structure at the level of monomer and chain packing under a variety of conditions. Experiments have shown that granular systems exhibit behavior characteristic of "traditional" polymer solids, such as a chain-length-dependent glass (jamming) transition [1] as well as strain hardening [2]. In parallel, simulations on athermal chain packings have shown other features shared by traditional polymeric systems, such as competing crystallization and glass transitions [6–11]. Crystal nucleation and growth in athermal chain packings share common features with their monomeric counterparts. Prominent among these is the formation of random hexagonal close-packed (rhcp) crystal morphologies of hexagonal close-packed (HCP) and face-centered cubic (FCC) crystallites. For fully flexible chains, monomers occupy the regular sites of crystallites, but chains maintain random-coil structure (as in the amorphous state [8–11]), rather than developing the extended conformations and lamellar morphologies possessed by traditional semicrystalline polymers [12]. In addition to the original granular polymers composed of metallic beads [1,2], softer colloidal polymers composed of polystyrene beads [4] have recently been synthesized. Inspired by these experimental and modeling developments, we propose a simplified thermal model to study crystallization in *soft* colloidal polymers.

A coarse-grained polymer model should include a minimal set of features necessary to capture the physical phenomena of interest, while remaining maximally computationally expedient. For example, the flexible Kremer-Grest (KG) bead-spring model [13] is a minimal model, including only chain connectivity, excluded volume and (in subsequent modifications [14]) van der Waals attractions. Despite this relative simplicity, it is able to capture the behavior of real polymers to an extraordinary degree, exhibiting features ranging from Rouse and entangled dynamics (i.e., reptation [15]) in its molten state [13,16] to dynamical heterogeneity in its glass transition regime [17] to aging, rejuvenation, and strain hardening in its amorphous glassy state [18–20]. One important feature of the standard KG model is that it possesses an inherent length-scale competition; the equilibrium length ℓ_0 of backbone bonds is significantly different from the equilibrium separation r_0 for nonbonded monomers. For long chains, this competition strongly promotes glass formation at the expense of crystallization [14]. While this inherent characteristic renders it an excellent tool to study glass-forming polymers, it is not directly applicable to simulations of chain crystallization.

More detailed, united atom (atomistic) models [21–24] exhibit crystallization [23–25], as well as glass formation [26], and incorporate the bond-angular and dihedral interactions required to map to specific polymer chemistries, but are computationally expensive and are inappropriate for modeling colloidal polymers. In the opposite limit, as described above, the simplest models treat polymers as freely jointed chains of tangent hard spheres with $\ell_0 = r_0$. These exhibit an entropically (free volume) driven crystallization transition [6–11]. One limitation of these latter, highly idealized models, however, is that they are athermal, while $k_B T$ is a critical parameter that should profoundly affect key properties of soft colloidal polymers. It is desirable, therefore, to develop simple polymer models that possess both the soft excluded volume and van der Waals interactions necessary to capture thermal behavior (in particular, exhibiting a glass transition) *and* a local chain structure amenable to crystallization, i.e., $\ell_0 = r_0$.

In this paper, we propose such a model and describe its basic properties. We will show that rapidly quenched systems remain largely amorphous down to $T = 0$, while slowly quenched systems display a degree of crystalline order that increases with decreasing quench rate $|\dot{T}|$. Consistent with results for athermal polymer packings [8–11], our model forms close-packed crystallites of FCC, HCP, or mixed FCC-HCP order with varying degrees of stacking faults and

*rshoy@usf.edu

five-fold-symmetric defects. We show that in the absence of chain stiffness, the condition that enforces $\ell_0 = r_0$ leads to crystal morphologies that closely resemble those encountered in athermal polymer packings and dense colloidal systems. The present model is thus suitable to study how parameters such as packing fraction and temperature (when decoupled from concomitant changes in chain conformation) dictate the formation of ordered morphologies in model colloidal polymers.

II. MODEL AND METHODS

Each polymer chain consists of $N = 50$ coarse-grained beads. All beads have mass m and all interact in pairs via the truncated and shifted Lennard-Jones (LJ) potential $U_{\rm LJ}(r) = 4u_0[(\sigma/r)^{12} - (\sigma/r)^6 - (\sigma/r_c)^{12} + (\sigma/r_c)^6]$, where u_0 is the intermonomer binding energy, $r_c = 2^{7/6}\sigma$ is the potential cutoff radius, and $U_{\rm LJ}(r) = 0$ for $r > r_c$. Bonds between successive beads along the chain backbone are modeled using a harmonic potential of the form $U_{\rm bond}(\ell) = (k_b/2)(\ell - \ell_0)^2$, where the equilibrium bond length ℓ_0 is set equal to the monomer diameter a and $k_b = 600u_0/a^2$. A key feature of the model is the condition that enforces the equilibrium bond length to be commensurate with the equilibrium nonbonded separation, i.e., $r_0 = \ell_0 = a$. This is achieved by setting $\sigma = 2^{-1/6}a$. We should further note that in contrast to the hard-core potential of the athermal representation in Refs. [8–10], overlaps between monomers can occur. The unit of time is $\tau = \sqrt{m\sigma^2/u_0}$; we employ a timestep $\delta t = \tau/300$. The maximal energetic barrier to chain crossing is $k_b(\sqrt{2}-1)^2a^2 \simeq 100u_0$, i.e., $\gtrsim 100k_BT$ for the systems considered here [27]. Cubic simulation cells consist of $N_{\rm ch} = 500$ chains for a total of $N_{\rm ch}N = 25\,000$ beads. Periodic boundary conditions are applied in all three directions. Initial melt states are generated with a monomer number density $\rho = 1.0a^{-3}$ (packing fraction $\phi = \pi\rho/6$). After thorough equilibration at $k_BT = 1.2u_0$, systems are quenched to zero temperature at various rates $|\dot{T}|$ while maintaining zero hydrostatic pressure using a (chainless) Nose-Hoover thermostat and barostat. The damping times of the thermostat and barostat are τ and 10τ, respectively. All simulations reported here are performed using LAMMPS [28]. Throughout the rest of the paper, we will express temperatures in units of k_BT/u_0, quench rates in units of τ^{-1}, distances in units of a, and densities in units of a^{-3}.

During the quenches, we monitor several quantities, including the potential energy per monomer U, the pair correlation function $g(r)$, the packing fraction ϕ, and metrics of local structure, including the characteristic crystallographic element (CCE) norm [8–10,29]. The later is a highly discriminating descriptor that quantifies the orientational and radial similarity of a local environment to a given ordered structure in atomic and particulate systems. The CCE norm is built around the defining set of crystallographic elements and the subset of distinct elements of the corresponding point symmetry group that uniquely characterize the reference crystal structure. For example, the FCC crystal symmetry is mapped onto a set of four threefold axes (roto-inversions of $2\pi/3$), while the HCP is mapped onto a single sixfold symmetry axis (roto-inversion of $\pi/3$). A scan in the azimuthal and polar angles identifies the set of axes that minimize the CCE norm of a reference site (atom or particle) with respect to a given crystal structure X. Details on the underlying mathematical formulas and the algorithmic implementation can be found in Ref. [29]. Once the CCE norm (ϵ_i^X) is calculated for each site i, an order parameter s^X can be calculated, which corresponds to the fraction of sites with CCE norms below a preset threshold value ($\epsilon_i^X \leqslant \epsilon^{\rm thres}$). Results from the CCE-norm-based analysis with respect to FCC, HCP, and fivefold symmetries are presented below.

III. RESULTS

Figure 1 illustrates the evolution of packing fraction $\phi(T)$ and potential energy $U(T)$ at various quench rates. To facilitate comparisons with experiment, we show both the "bare" $\phi(T)$ [Fig. 1(a)] and an effective packing fraction $\phi_{\rm eff}(T)$. The latter is obtained by setting an effective hard-sphere radius equal to the inner monomer radius $r_{\rm eff}$, where the LJ potential is equal to k_BT, i.e., $\phi_{\rm eff} = (r_{\rm eff}/a)^3\phi$, where $U_{LJ}(r_{\rm eff}) - U_{LJ}(a) = k_BT$. For slow quench rates, the data show clear signatures of a phase transition (crystallization) at $T_{\rm cryst} \simeq 0.56$; ϕ (U) exhibit upward (downward) jumps that indicate an increasingly first-order-like transition as $|\dot{T}|$ decreases. For the fastest quench rate, ϕ and U show no apparent signs of crystallization; a weak glass transition, as indicated by a smooth bend in U and ϕ, is observed at $T = T_g \simeq 0.45$. As in traditional semicrystalline polymers, $T_{\rm cryst} > T_g$. Note that in contrast to recent work on athermal systems [6,7], our model does not "jam" at random close packing ($\phi_{\rm RCP} = 0.636$ [30]) even for

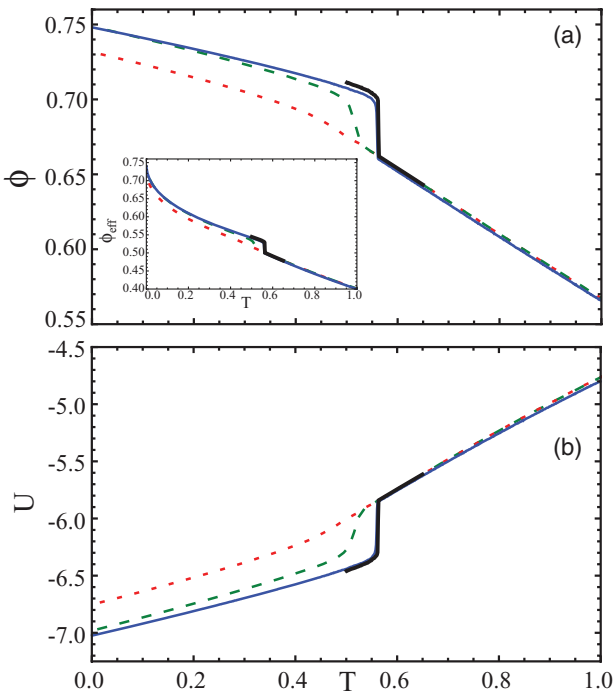

FIG. 1. (Color online) Volumetric and energetic measures of the crystallization transition. Heavy solid, light solid, dotted, and dashed lines show data for $|\dot{T}| = 10^{-7}$, $|\dot{T}| = 10^{-6}$, $|\dot{T}| = 10^{-5}$, and $|\dot{T}| = 10^{-4}$, respectively. Panel (a) illustrates the packing fraction ϕ and panel (b) illustrates the potential energy per monomer U, while the inset to panel (a) illustrates $\phi_{\rm eff}$. For the slowest quench rates, both data sets indicate $T_{\rm cryst} \simeq 0.56$.

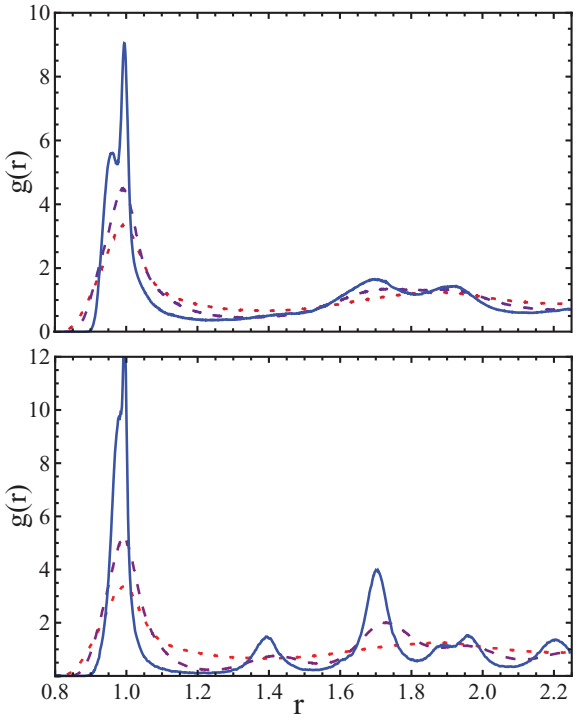

FIG. 2. (Color online) Pair radial correlation function, $g(r)$ at various temperatures and cooling rates. Dotted, dashed, and solid lines show data for $T = 1.0$, 0.5, and 0, respectively. The top panel shows data for $|\dot{T}| = 10^{-4}$, while the bottom panel shows data for $|\dot{T}| = 10^{-6}$.

the fastest studied quench rate. Also note that the cooling at rate $|\dot{T}| = 10^{-7}$ is terminated at $T = 0.5$ due to the limits of current computational resources. We find no major qualitative differences between results obtained at the two lowest quench rates (cf. Fig. 4).

Figure 2 shows the evolution of the pair radial correlation function $g(r)$ with T at the slowest and fastest $|\dot{T}|$. Results are reported for temperatures well above the melting point, slightly below $T_{\rm cryst}$, and zero. Above the melting point, systems have amorphous (melt-like) structure as expected. For slow quenches, just below $T_{\rm cryst}$, peaks in the correlation function are formed corresponding to the appearance and growth of close-packed order. At zero temperature, clear peaks at the characteristic second- and third-nearest-neighbor distances for close-packed crystals, $r_{2n} = \sqrt{2}$ and $r_{3n} = \sqrt{3}$ have developed [31]; the system also retains some amorphous character as indicated by the large width of these peaks. In sharp contrast, for the fastest quench rate $|\dot{T}| = 10^{-4}$, systems at the same temperatures remain predominantly amorphous; $g(r)$ maintains liquid-like structure down to $T = 0$. Note that the first peak of $g(r)$ is rather broad and occurs at pair distances slightly smaller than bead diameter a due to the attractive tail of the LJ potential. An iterative process of reducing ℓ_0 to match the $r_{\rm nn}$ obtained at $T = 0$ could presumably result in even more pronounced ordering than that reported below.

We now turn to a detailed examination of the local environment around each monomer and to the identification of crystalline structure (or the lack thereof) as a function of T for various quench rates. As described in the above, we

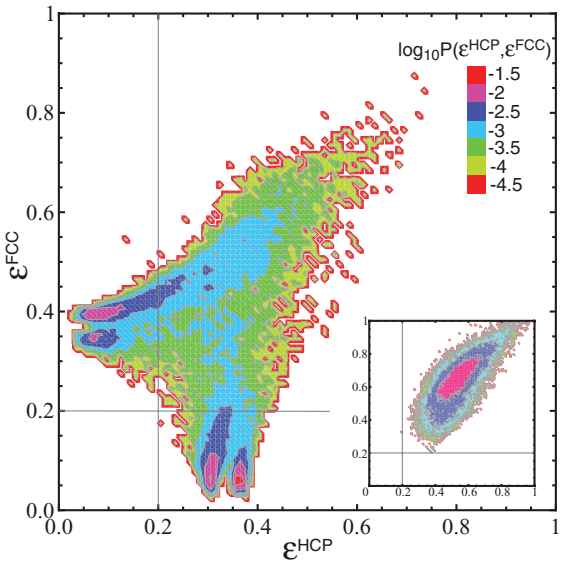

FIG. 3. (Color online) Parity plot of the $\epsilon^{\rm FCC}$ versus $\epsilon^{\rm HCP}$ CCE-based norms over all monomers for $|\dot{T}| = 10^{-6}$ at $T = 0$ and (inset) $T = 1.0$. Colors (scales of gray) indicate the (log-scale) site ordering probability density $P(\epsilon^{\rm HCP},\epsilon^{\rm FCC})$. Horizontal and vertical gray lines indicate the threshold value of the CCE norm ($\epsilon^{\rm thres} = 0.20$). Note that the vacancy of the region defined by $(\epsilon^{\rm FCC}, \epsilon^{\rm HCP}) < (0.2, 0.2)$ highlights the discriminating character of the CCE descriptor.

have implemented the CCE norm to identify HCP, FCC, and fivefold structures. The highly discriminating nature of the CCE norm is demonstrated in Fig. 3, where parity plots [29] for the HCP and FCC-CCE norms are shown for $|\dot{T}| = 10^{-6}$ at $T = 1.0$, where the system is amorphous, and at $T = 0$, where it becomes predominantly ordered. Sites with HCP- (or FCC-) CCE norms with values lower than $\epsilon^{\rm thres} = 0.20$ are characterized as HCP-like (or FCC-like). By construction, a monomer with high HCP similarity (i.e., low HCP-CCE norm) possesses low FCC similarity (high value of FCC-CCE norm) and vice versa. Thus, for any system configuration we can reliably identify the local environment around each monomer with respect to HCP, FCC, and fivefold symmetries. The figure illustrates that in the liquid state at $T = 1.0$, essentially no monomers have local FCC or HCP order, while at zero temperature, a large fraction of sites (∼65%) possess either FCC or HCP order, with comparable probability. The remaining 35% of sites have either fivefold or "other" local structure, as indicated by the region $(\epsilon^{\rm FCC}, \epsilon^{\rm HCP}) > (0.2, 0.2)$. As we will show below, this noncrystalline portion of samples consists mainly of stack-faulted domain walls and/or an amorphous interphase.

Next, we present results, based on the CCE analysis, on the evolution of local ordering with decreasing T. Figure 4 shows the fraction of sites with: (a) close-packed (FCC or HCP) order, (b) fivefold similarity, and (c) neither fivefold local symmetry nor close-packed order, as a function of T, for different quench rates. In all cases, close-packed ordering grows continuously as T decreases, with the transition at $T = T_{\rm cryst}$ becoming increasingly first-order-like with decreasing $|\dot{T}|$. As T drops further, the fraction of close-packed sites continues to increase, indicating an effective "annealing" process, wherein structural

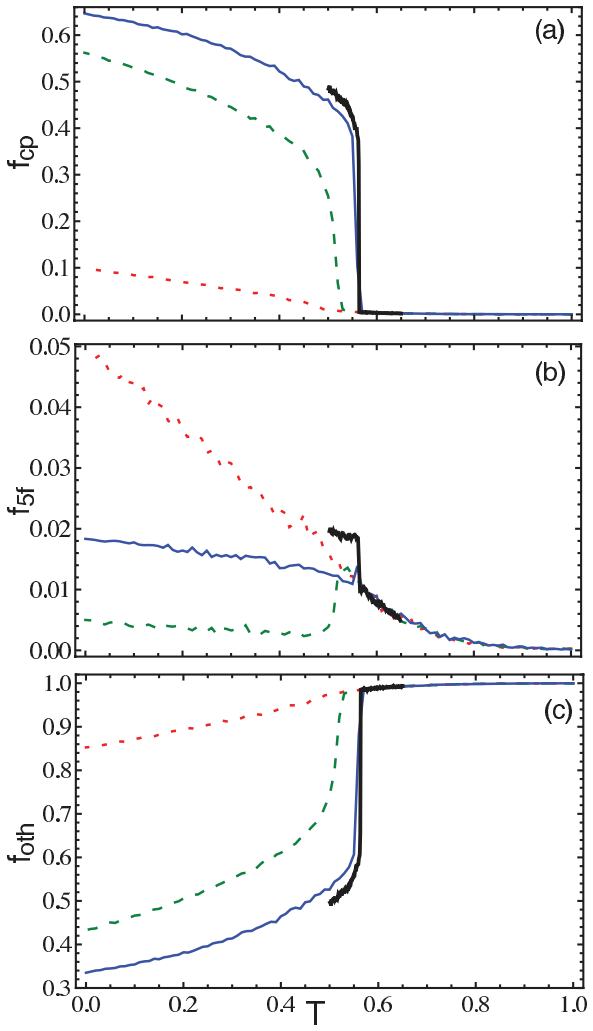

FIG. 4. (Color online) Measures of crystalline order versus T at various quench rates. Heavy solid, light solid, dotted, and dashed lines show data for $|\dot{T}| = 10^{-7}$, $|\dot{T}| = 10^{-6}$, $|\dot{T}| = 10^{-5}$, and $|\dot{T}| = 10^{-4}$, respectively. Panel (a), fraction of sites f_{cp} with close-packed order; panel (b), fraction of sites f_{5f} with fivefold local symmetry; panel (c), fraction of sites f_{oth} with other local structure.

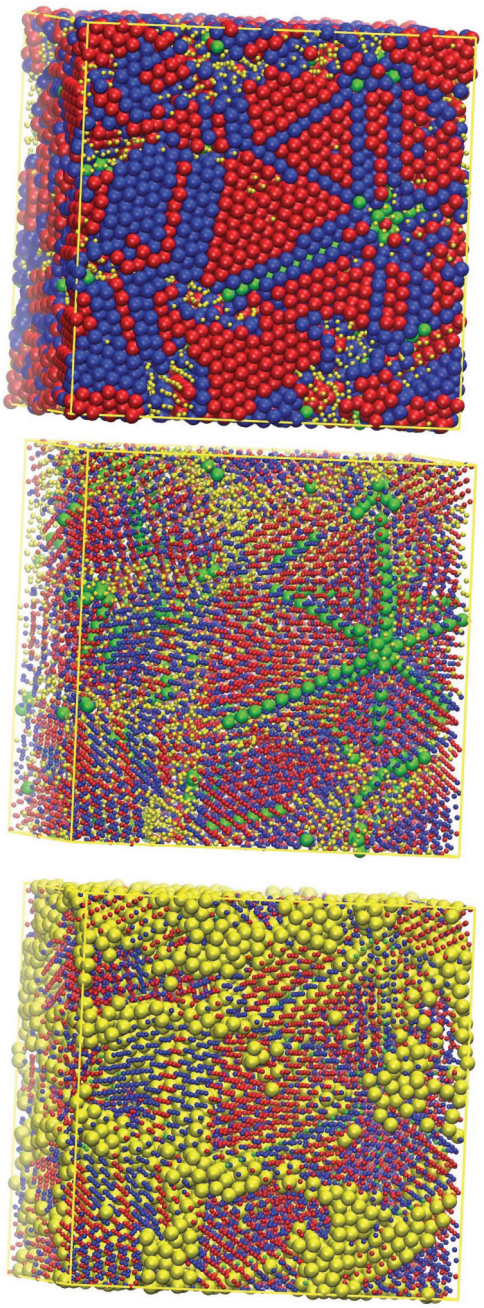

FIG. 5. (Color online) Snapshot of system quenched at $|\dot{T}| = 10^{-6}$, at $T = 0$. (Top panel) HCP-ordered sites are shown in blue (dark gray), FCC-ordered sites in red (medium gray), fivefold sites in green (light gray), and "other" sites in yellow (very light gray). The diameter of "other" sites is scaled in 1:3 ratio for clarity purposes. (Middle panel) Same coloring scheme as in top panel, but with the diameters of the HCP, FCC, and "other" sites scaled in 1:3 ratio. (Bottom panel) Same coloring scheme as in top panel, but with the diameters of the HCP, FCC, and fivefold sites scaled in 1:3 ratio. Image created with the VMD software [40].

defects are removed. Throughout this process, the fraction of sites with FCC order is comparable to but exceeds the fraction of sites with HCP order, especially at the slowest $|\dot{T}|$. This is expected, since while the free-energy difference between the FCC and HCP phases for the Lennard-Jones potential is very small [32], crystal-growth kinetics favor FCC crystallite formation [33].

The fraction of sites with close-packed order, f_{cp}, increases sharply with decreasing quench rate for T slightly below T_{cryst} and continues to increase as T decreases to zero. For example, at $T = 0$, f_{cp} is only 10% for $|\dot{T}| = 10^{-4}$ but rises to 58% for $|\dot{T}| = 10^{-5}$ and to 65% for $|\dot{T}| = 10^{-6}$. At the intermediate quench rate, the jumps in U, ϕ, and f_{cp} all exhibit a "delay" to $T \simeq .52$, indicating a critical nucleation rate of $|\dot{T}|_{crit} \simeq 10^{-5\pm1}$. Quench-rate-dependent differences in crystal structure for $T = 0$ will be examined in more detail below.

Fivefold local symmetry is well-known to inhibit crystallization and promote amorphous structure in numerous physical systems [34–39]. Thus, it is particularly interesting to study how fivefold similarity evolves during the cooling simulations of the present coarse-grained polymer model. For all quench rates, as density (ϕ) increases for $T > T_{cryst}$, so does the population of sites with fivefold symmetry. This trend is

consistent with results from simulations on monomeric hard spheres of uniform size [39] where fivefold probability in amorphous athermal packings increases as the system becomes denser. The physical behavior changes drastically as temperature reaches and drops below T_{cryst}. For the fastest quench rate, f_{cp} continues to grow linearly and the system remains amorphous with only a small fraction of ordered sites. In sharp contrast, the population of fivefold sites drops significantly for $|\dot{T}| = 10^{-5}$, remains nearly constant for $|\dot{T}| = 10^{-6}$, and exhibits a small upward jump (but one within statistical, sample-to-sample variations) for $|\dot{T}| = 10^{-7}$. These findings clearly point toward a structural competition between close-packed ordering and fivefold symmetry (e.g., twin defects). While this competition has been observed in a wide range of athermal polymeric as well as colloidal packings [35–39], it is the first demonstration of such structural competition in more detailed, thermal polymer models.

Many sites lack either close-packed order or fivefold similarity; Fig. 4(c) shows the fraction of such sites, $f_{\text{oth}} = 1 - f_{\text{cp}} - f_{5f}$. We note that $f_{\text{oth}} \simeq 1$ above T_{cryst}, indicating that for the CCE-norm structure-identification procedure described above, f_{oth} is a good discriminant of liquid-like order. For $|\dot{T}| > |\dot{T}|_{\text{crit}}$, systems retain amorphous structure down to $T = 0$, consistent with the $g(r)$ data shown in Fig. 2. For $|\dot{T}| < |\dot{T}|_{\text{crit}}$, f_{oth} shows a first-order-like (downward) jump at $T = T_{\text{cryst}}$ and continues to decrease with decreasing T during crystal healing but remains significant down to $T = 0$.

Visualization of systems prepared at various $|\dot{T}|$ provides considerable insight into the semicrystalline morphologies formed by the present chain model. Figure 5 shows the end state ($T = 0$) for $|\dot{T}| = 10^{-6}$. Grain-like HCP and FCC domains are clearly visible along with fivefold-symmetric sites. The later are strongly related to twinning planes at crystalline boundaries as found in polycrystalline metallic or colloidal systems [41] and in dense packings of monomeric hard spheres [38,39]. The ordered structures, as established here, show reduced tendency to layer formation (randomly stacked hexagonal close packing) compared to that found for hard-sphere chains in Refs. [8–10], presumably because the larger system sizes employed here reduce the influence of the periodic boundaries or because in the athermal systems a strict tangency condition is applied with respect to the fluctuation of bond lengths. Still, it is interesting that the present *thermal* model shows a crystallization pattern that is strikingly similar with the one observed in dense packings of freely jointed chains of hard spheres [8–11]. Careful visual inspection of the "other" sites shows that such clusters and regions possess nearly close-packed structure and correspond to stack-faulted domain walls. Since the crystallite domain size is considerably smaller than our simulation cells, these domain walls form a percolating structure.

Faster quench rates produce reduced crystalline order and a correspondingly more amorphous structure. Figure 6 shows the ($T = 0$) end state of a system quenched at $|\dot{T}| = 10^{-4}$. HCP and FCC crystallites are present but are far smaller and fewer. Furthermore, the crystallite/grain-boundary structure reported earlier is absent. The number of fivefold sites is much greater and these sites, rather than corresponding to twin

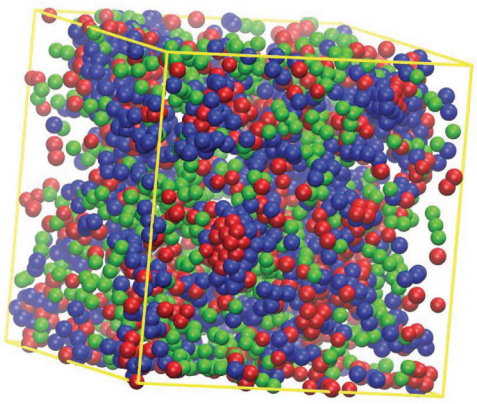

FIG. 6. (Color online) Snapshot of system quenched at $|\dot{T}| = 10^{-4}$, at $T = 0$. HCP-ordered sites are shown in blue (dark gray), FCC-ordered sites in red (medium gray), and fivefold sites in green (light gray). Image created with the VMD software [40].

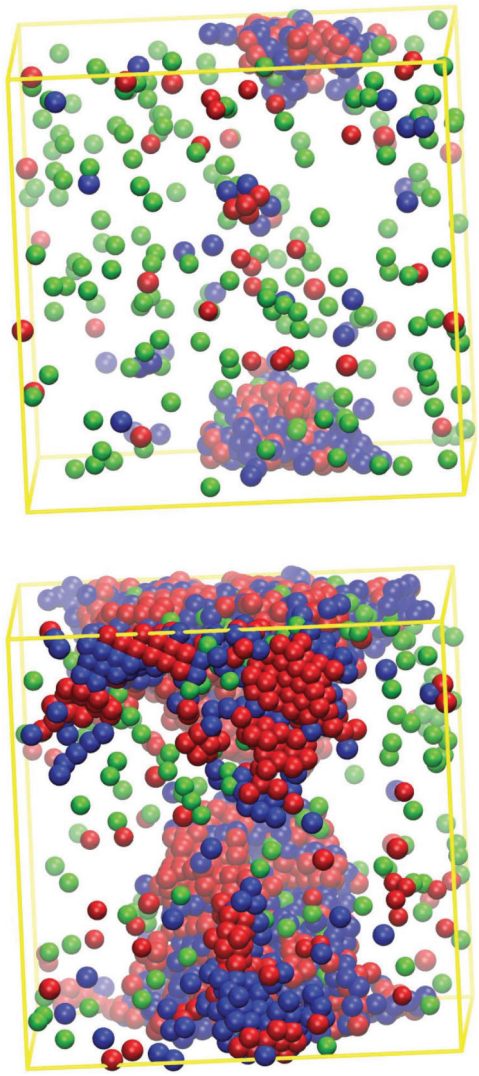

FIG. 7. (Color online) Crystal nucleation at $|\dot{T}| = 10^{-6}$. (Top) Formation of a small nucleus at $T = .562$. (Bottom) Growth of nucleus: $T = 0.561$. The systems have $f_{\text{cp}} = 0.019$ and 0.14, respectively. HCP-ordered sites are shown in blue (dark gray), FCC-ordered sites in red (medium gray), and fivefold sites in green (light gray). Image created with the VMD software [40].

defects, are apparently arranged randomly. Visual inspection of the "other" sites for this quench rate shows that they are much less ordered than those for the lowest quench rate, in effect corresponding to an amorphous interphase. Thus, our model is able to produce large crystallites with domain walls for slow quench rates and a predominantly amorphous structure with small crystallites for fast ones. For $|\dot{T}| = 10^{-5} \simeq |\dot{T}|_{\rm crit}$, results are intermediate between these two limiting cases, with a tendency toward the crystalline state.

Finally, significant information on crystal nucleation and growth can be obtained by visual examination of the polymer system as it evolves in the vicinity of $T \simeq T_{\rm cryst}$. Figure 7 shows a pair of snapshots from the $|\dot{T}| = 10^{-6}$ quench. At $T = 0.562$, the first trace of crystal aggregates can be seen in the form of a small nucleus, which consists of similar amounts of HCP and FCC sites. As the system is still amorphous, the number of sites with fivefold symmetry is comparable to the fraction of sites with either HCP or FCC similarity. However, by $T = 0.561$, the number of ordered sites present in the system has greatly increased and the first large crystal nucleus is extant, consisting again of roughly equal amounts of HCP- and FCC-like sites. As T continues to drop, this nucleus continues to grow and expand until it fills most of the system as illustrated in Fig. 5.

IV. DISCUSSION AND CONCLUSIONS

Inspired by recent modeling advances in the crystallization of athermal chain packings and experimental developments in granular and colloidal polymers, we have studied a minimal model for the packing and crystallization of "soft" colloidal polymers [4]. Crystallization is promoted by removing the length-scale competition present in the Kremer-Grest bead-spring model [13]. By employing refined descriptors of local structure, we are able to identify and track the evolution of order as a function of temperature and quench rate. At fast quench rates, chain systems remain predominantly amorphous with a large number of fivefold-symmetric sites, typifying quenched-disorder vitrification. At slow quench rates, the system exhibits a first-order phase transition wherein crystal nuclei form in coexistence with an amorphous phase. Since our model employs fully flexible chains and possesses a backbone bond length that is commensurate with the nonbonded separation distance, it forms close-packed crystallites of FCC, HCP, or mixed FCC/HCP order, separated by grain boundaries. These morphologies closely resemble the ones encountered in the crystallization of dense athermal polymer packings [8–11] and generally in the crystallization of colloidal systems.

In stark contrast with traditional polymer systems, but in agreement with studies of flexible granular chains, crystallization in the present model does not entail formation of lamellar structures. As in studies of athermal models, the absence of angular interactions reduces or eliminates any thermodynamic driving forces that would produce the formation of lamellae. We find no increase in conformational persistence, i.e., no chain uncoiling, during cooling at any of the studied quench rates. Instead, chains contract nearly affinely (in $\phi^{-1/3}$) at large scales during densification. Thus, our current model is well suited to studies that isolate the role of packing fraction (i.e., by decoupling it from concomitant changes in chain conformation) on the dynamics and thermodynamics of densely packed chains.

Our model is comparable to the CG-PVA model [23,24], which has been used to study generic features of traditional polymer crystallization such as lamella formation and chain disentanglement [42] during the crystallization process. The CG-PVA model differs from ours primarily via its employment of a stiff angular potential specific to PVA, purely repulsive pair interactions, and overlap between covalently bonded beads. The latter feature is appropriate for the study of crystallization of traditional polymers but not for colloidal or granular polymers [1,2,4], which typically lack interbead overlap.

Key advantages of the present model over the previous athermal models include realistic dynamics and straightforward accounting for thermal effects. It can be employed to study in systematic fashion the effect of different chain topologies (branched polymers, H-polymers, stars, etc.) and chain stiffness on crystal nucleation and growth. Such simulations could be executed without the need to develop advanced Monte Carlo techniques. As described in the Appendix, adding a generic angular potential to our model produces lamellar-like ordering in the crystalline state. Future work will: (i) investigate the effect of generic angular and torsional potentials on crystal structure and lamella-formation [43,44], and (ii) examine the effect of different chain topologies (i.e., branching) on crystal nucleation and growth. Such studies are expected to answer fundamental questions on the factors affecting the formation of ordered morphologies in dense colloidal chain packings.

ACKNOWLEDGMENTS

We are grateful to Manuel Laso and Katerina Foteinopoulou (UPM, Spain) for fruitful discussions on polymer crystallization. Tyler Smith provided assistance with VMD. N.C.K. acknowledges support by the Spanish Ministry of Economy and Competitiveness (MINECO) through Projects No. "I3" and No. MAT2010-15482, as well as the computer resources, technical expertise, and assistance provided by the Centro de Supercomputacion y Visualizacion de Madrid (CeSViMa).

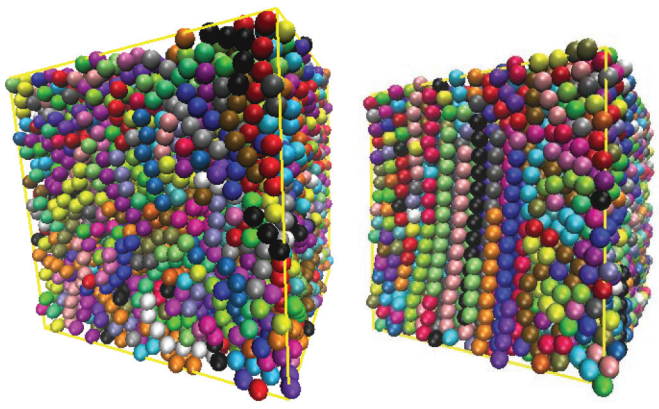

FIG. 8. (Color online) Formation of lamellae for semiflexible chains. The left and right panels show system configurations at $T = 1.0$ and $T = 0.2$, respectively. Different colors indicate different chain molecules. Image created with the VMD software [40].

APPENDIX: EXTENSION TO SEMIFLEXIBLE CHAINS

While the focus of this paper is on fully flexible chains, we emphasize that our model is easily extensible to semiflexible chains. We add an angular potential $U_\theta = k_{\rm bend}[1 + \cos(\theta)]$, where $\cos(\theta_i) = (\vec{b}_i \cdot \vec{b}_{i+1})/(\|\vec{b}_i\|\|\vec{b}_{i+1}\|)$ and the bond vector $\vec{b}_i = \vec{r}_{i+1} - \vec{r}_i$. Figure 8 illustrates ordering in systems of $N_{\rm ch} = 500$ chains of length $N = 13$, above and below $T_{\rm cryst}$ for $k_{\rm bend}/u_0 = 7$. Nematic interchain alignment typical of lamellar precursors for short chains is clearly present in the ordered state at low temperature. Future work will examine the factors affecting lamellae formation and in particular the transition from random-walk-like to lamellar chain ordering with increasing $k_{\rm bend}$.

[1] L.-N. Zou, X. Cheng, M. L. Rivers, H. M. Jaeger, and S. R. Nagel, Science **326**, 408 (2009).
[2] E. Brown, A. Nasto, A. G. Athanassiadis, and H. M. Jaeger, Phys. Rev. Lett. **108**, 108302 (2012).
[3] L. M. Lopatina, C. J. Olson Reichhardt, and C. Reichhardt, Phys. Rev. E **84**, 011303 (2011).
[4] H. R. Vutukuri, A. F. Demirors, B. Peng, P. D. J. van Oostrum, A. Imhof, and A. van Blaaderen, Angew. Chem. Int. Ed. **51**, 11249 (2012).
[5] I. Coluzza, P. D. J. van Oostrum, B. Capone, E. Reimhult, and C. Dellago, Phys. Rev. Lett. **110**, 075501 (2013).
[6] N. C. Karayiannis and M. Laso, Phys. Rev. Lett. **100**, 050602 (2008).
[7] N. C. Karayiannis, K. Foteinopoulou, and M. Laso, J. Chem. Phys. **130**, 164908 (2009).
[8] N. C. Karayiannis, K. Foteinopoulou, and M. Laso, Phys. Rev. Lett. **103**, 045703 (2009).
[9] N. C. Karayiannis, K. Foteinopoulou, C. F. Abrams, and M. Laso, Soft Matter **6**, 2160 (2010).
[10] N. C. Karayiannis, K. Foteinopoulou, and M. Laso, Int. J. Mol. Sci. **14**, 332 (2013).
[11] R. Ni and M. Dijkstra, Soft Matter **9**, 365 (2013).
[12] I. M. Ward and J. Sweeney, *An Introduction to the Mechanical Properties of Solid Polymers* (John Wiley & Sons, New York, 2004).
[13] K. Kremer and G. S. Grest, J. Chem. Phys. **92**, 5057 (1990).
[14] C. Bennemann, W. Paul, K. Binder, and B. Dünweg, Phys. Rev. E **57**, 843 (1998).
[15] M. Doi and S. F. Edwards, *The Theory of Polymer Dynamics* (Clarendon Press, Oxford, 1986).
[16] M. Pütz, K. Kremer, and G. S. Grest, Europhys. Lett. **49**, 735 (2000).
[17] Y. Gebremichael, T. B. Schroder, F. W. Starr, and S. C. Glotzer, Phys. Rev. E **64**, 051503 (2001).
[18] J. Rottler and M. O. Robbins, Phys. Rev. Lett. **95**, 225504 (2005).
[19] R. S. Hoy and M. O. Robbins, J. Polym. Sci. Part B: Polym. Phys. **44**, 3487 (2006).
[20] M. Warren and J. Rottler, Phys. Rev. E **76**, 031802 (2007).
[21] J. P. Ryckaert and A. Bellemans, Faraday Discuss. **66**, 95 (1978).
[22] S. Toxvaerd, J. Chem. Phys. **93**, 4290 (1990).
[23] H. Meyer and F. Müller-Plathe, J. Chem. Phys. **115**, 7807 (2001).
[24] H. Meyer and F. Müller-Plathe, Macromolecules **35**, 1241 (2002).
[25] C. Liu and M. Muthukumar, J. Chem. Phys. **109**, 2536 (1998).
[26] P. V. K. Pant, J. Han, G. D. Smith, and R. H. Boyd, J. Chem. Phys. **99**, 597 (1993).
[27] This is obtained by assuming chains cross at 90° angles and bonds are stretched to a length $\ell = \sqrt{2}$. A smaller energy barrier $\sim 40u_0$ could be obtained by considering the softness of the LJ interactions, but this is still of order $60\,k_BT$ or greater for the temperatures of primary interest here.
[28] S. Plimpton, J. Comp. Phys. **117**, 1 (1995).
[29] N. C. Karayiannis, K. Foteinopoulou, and M. Laso, J. Chem. Phys. **130**, 074704 (2009).
[30] S. Torquato, T. M. Truskett, and P. G. Debenedetti, Phys. Rev. Lett. **84**, 2064 (2000).
[31] Note the slight double peak at $r \sim 1$ in Fig. 2 arises because of the slight stiffness mismatch between pair and bond interactions.
[32] P. G. Bolhuis, D. Frenkel, S. C. Mau, and D. A. Huse, Nature (London) **388**, 235 (1997).
[33] B. W. van de Waal, Phys. Rev. Lett. **67**, 3263 (1991).
[34] F. C. Frank, Proc. Roy. Soc. London. Ser. A **215**, 43 (1952).
[35] J. Russo and H. Tanaka, Sci. Rep. **2**, 505 (2012).
[36] M. Leocmach and H. Tanaka, Nat. Commun. **3**, 974 (2012).
[37] J. Taffs, S. R. Williams, H. Tanaka, and C. P. Royall, Soft Matter **9**, 297 (2013).
[38] N. C. Karayiannis, R. Malshe, J. J. de Pablo, and M. Laso, Phys. Rev. E **83**, 061505 (2011).
[39] N. C. Karayiannis, R. Malshe, M. Kröger, J. J. de Pablo, and M. Laso, Soft Matter **8**, 844 (2012).
[40] W. Humphrey, A. Dalke, and K. Schulten, J. Mol. Graphics **14**, 33 (1996).
[41] B. O'Malley and I. Snook, Phys. Rev. Lett. **90**, 085702 (2003).
[42] C. Luo and J.-U. Sommer, ACS Macro. Lett. **2**, 31 (2013).
[43] T. Vettorel, H. Meyer, J. Baschnagel, and M. Fuchs, Phys. Rev. E **75**, 041801 (2007).
[44] M. Bernabei, A. J. Moreno, and J. Colmenero, J. Chem. Phys. **131**, 204502 (2009).